Trends in vacancy distribution and hardness of high temperature neutron irradiated single crystal tungsten

G. Bonny[*1], M.I. Konstantinovic[1], A. Bakaeva[1], Y. Chao[1], N. Castin[1], K. Mergia[2], V. Chatzikos[2], S. Dellis[2], T. Khvan[1], A. Bakaev[1], A. Dubinko[1], D. Terentyev[1]

[1] SCK CEN, Nuclear Materials Science Institute, Boeretang 200, B-2400 Mol, Belgium

[2] National Centre for Scientific Research "Demokritos", Institute of Nuclear and Radiological Science and Technology, Energy and Safety, 15341 Agia Paraskevi, Athens, Greece

Abstract

The aim of the present study is to extend the knowledge about the formation and thermal stability of vacancy-type defects in tungsten under neutron irradiation, thereby mimicking the temperature and neutron flux expected in the ITER divertor. Neutron irradiation of single crystal tungsten, W(100), in the temperature range 600-1200 °C is performed up to 0.12 dpa. Positron annihilation spectroscopy is employed to detect the presence of open volume defects, while hardness tests are applied to relate the irradiation-induced defects with the modification of mechanical properties. Rationalization of the experimental results is enhanced by the application of a kinetic Monte Carlo simulation tool, applied to model the microstructural evolution under the neutron irradiation process. The relation between radiation microstructure and hardness is explained via a dispersed barrier model.

1. Introduction

Electricity produced by nuclear fusion reaction is considered as a complementary energy source to reduce fossil fuel consumption after 2050 [1]. Extraction of thermal energy by using thermo-nuclear fusion implies transfer of the kinetic energy of reaction neutrons to surrounding materials, thereby converting it into heat. Thus, the materials operating in a nuclear fusion environment are exposed to a high heat and fast neutron flux simultaneously.

[*] Corresponding author. Email: gbonny@sckcen.be; giovanni.bonny@gmail.com

Under irradiation by fast neutrons, materials exhibit modification of their properties, namely: their thermal, physical and mechanical properties degrade [2]. Among the different types of fusion reactor designs, the Tokamak has a high potential for commercialization, and it therefore serves as the main concept for DEMO (DEMOnstration Power Station) and ITER (International Thermonuclear Experimental Reactor) [3]. For both of these fusion facilities, tungsten is selected as primary candidate armor material for the plasma facing components.

The expected operational conditions of DEMO and ITER will lead to thermal shock, thermo-mechanical fatigue and radiation embrittlement in the first wall materials [4]. The choice of tungsten (W) is thus determined by its high melting point, low erosion rate, high thermal conductivity and resistance to thermal stresses [5]. One of the main caveats of W is its intrinsically high ductile to brittle transition temperature (DBTT), being around 200-400 °C (depending on the production route, purity and testing standard) [6]. Fast neutron exposure leads to the creation and accumulation of lattice defects, which obstruct plasticity, and therefore the DBTT of W will raise even further under operation [7-9].

Indeed, the point defects and their clusters created in atomic cascades diffuse and coalesce to form voids and dislocation loops, the two main types of neutron irradiation-induced microstructural defects [10]. Both voids and loops pin the dislocation movement at the nano-scale [11-13] and will therefore cause stress concentrations at the meso-scale and embrittlement at the macro-scale [8]. In addition, the development of voids results in the reduction of thermal conductivity [14, 15], which suppresses the heat transfer and enhances the risk of overheating of the plasma facing components.

In addition to the fast neutron flux, the penetration of energetic particles (i.e. hydrogen isotopes and helium) also have important consequences on the performance of the plasma facing components. In addition, the accumulation of tritium in the plasma facing components has a direct impact on the balance of plant (fuel supply) and safety margins on the tritium retention inside the in-vessel components [4]. Thereby the diffusion and retention of these energetic particles is governed by the concentration and morphology of irradiation-induced vacancies and vacancy clusters [16, 17].

Because of all the above, the understanding of the evolution of radiation defects and vacancy-type defects in particular, is critical for the assessment of the impact of fusion operational conditions on the performance of W in terms of ductile deformation, fracture toughness, thermal conductivity and tritium retention.

The experimental investigation of vacancy-type defects involves two complimentary methods: transmission electron microscopy (TEM) and positron annihilation spectroscopy

(PAS). In the literature, many works are available studying the neutron irradiation-induced microstructure via TEM in various tungsten grades [10, 18-26]. For irradiation temperatures below ~400 °C, mostly dislocation loops are observed, while above this temperature, both voids and loops are observed. Around the irradiation temperature of ~800 °C and above, the irradiation-induced microstructure is dominated by voids, rather than by loops. With increasing irradiation dose, the produced transmutation products, i.e., mostly Re and Os, cluster together to form non-cohesive sigma- and chi phase precipitates [27, 28].

In the literature, many works are available applying PAS to characterize the effects of ion irradiations, including He and/or H isotope implantation [29-37]. However, few works [38-40] are available where the neutron irradiation-induced microstructure was studied by PAS. In the works by Taylor et al [39, 40], neutron irradiated W samples (0.025-0.03 dpa) were exposed to a deuterium plasma in the temperature range 100-500 °C and various stages of radiation damage and deuterium retention were characterized. In the work by Hu et al [38], the effects of post-irradiation annealing on low-dose (0.006-0.03 dpa) low-temperature (~90 °C) neutron irradiated single crystal W were studied.

The aim of the present study is to extend the knowledge about the formation and thermal stability of vacancy-type defects in tungsten under neutron irradiation, thereby mimicking the temperature and neutron flux expected in the ITER divertor. Neutron irradiation of single crystal tungsten, W(100), in the temperature range 600-1200 °C is performed up to 0.12 dpa. Positron annihilation spectroscopy is employed to detect the presence of open volume defects, while hardness tests are applied to relate the irradiation-induced defects with the modification of mechanical properties. Rationalization of the experimental results is enhanced by the application of a kinetic Monte Carlo simulation tool, applied to model the microstructural evolution under the neutron irradiation process. The relation between radiation microstructure and hardness is explained via a dispersed barrier model.

Following this introduction, in **section 2** the used experiment and simulation methods are described. In **section 3**, the results obtained from PAS, micro-hardness and object kinetic Monte Carlo simulations are presented. In **section 4**, the measured and simulated radiation microstructure is linked to the measured radiation hardening, and apparent inconsistencies between the different data sets rationalized. In **section 5**, the global conclusions are summarized.

2. Experiment and Simulation Methods

2.1. Material and Irradiation Conditions

The single crystal tungsten, W(100), used in this study was produced by MaTeck (Germany) in a form of cylindrical rod with 12 mm diameter. The nominal purity of the material was 99.999%. Disc shaped specimens of about 0.8 mm thickness were cut using electric discharge machining (EDM) and subsequently polished to remove EDM damage. A mirror-like surface was achieved before the samples were placed in the irradiation rig. After neutron irradiation, optical imaging confirmed that the surface kept its good quality (i.e. no traces of mechanical damage or oxidation) after the irradiation.

Neutron irradiation was performed in the Belgian Reactor 2 (BR2) in Mol, Belgium. The irradiation rig was placed inside a fuel element to maximize the fast-to-thermal neutron ratio. This was done to reduce the transmutation rate of W into Re and Os, which is higher than expected in a fusion irradiation environment. The samples were located in the central part of the reactor core, where the maximum fast neutron (> 0.1 MeV) flux could reach up to 7×10^{14} $n\cdot cm^{-2}\cdot s^{-1}$.

During the irradiation, the samples were under a helium inert atmosphere and the nominal irradiation temperatures were 600, 800, 900 and 1200 °C following thermal and neutronic calculations. The irradiation dose was 0.12 displacement per atom (dpa), as calculated by MCNPX 2.7.0, based on the total fast neutron fluence calculated post factum [41].

The dpa cross sections for W were prepared from the JENDL4 file (MT444) for the threshold displacement energy of 55 eV, following the recommendation by IAEA [42, 43]. The transmutation of Re and Os was calculated based on the ALEPH code developed at SCK CEN and available nuclear databases [44, 45]. For the irradiation position of the samples, 0.25-0.33 at.% Re and 0.07-0.10 at.% Os was produced via transmutations.

In addition to neutron irradiation, electron irradiation was performed on recrystallized tungsten foils with the purpose of inducing a controlled concentration of vacancies and assess their effects on the positron annihilation spectroscopy (PAS) measurements. A commercially pure (99.99%) tungsten foil of 100 μm thickness was supplied by Plansee (Austria) and the foil was annealed at 1600 °C for 1 hour in an inert atmosphere. After the annealing, the grain size of the foil reached about 500 μm, and most of the grains had a <110> orientation (as expected based on the surface energy minimization). Thus, the samples exposed to the electron irradiation could be considered as single crystals.

Electron irradiation was performed at the Moscow National Research Nuclear University (Mephi) using 3.5 MeV electrons and a current of 40 $\mu A/cm^2$, with a flux of 2.5×10^{14}

e^- $cm^{-2} \cdot s^{-1}$. The irradiated samples had the dimension $10 \times 10 \times 0.1$ mm^3 and a stack of two samples (stacked normal to the beam) was irradiated for 5 hours. Two stacks were irradiated to provide three pairs of samples required to perform PAS analysis. The number of displacement events was calculated using cross sections taken from [46]. Given the uncertainty in the threshold displacement energy (55-90 eV) a range for the concentration of point defects was assessed for the two samples located in the stack as: 30-60 appm for the first 100 μm layer and 10-20 appm for the second layer. The irradiation was performed at room temperature and the holder had active cooling at the back side to avoid overheating of the samples. In such irradiation conditions, 3.5 MeV electrons produce solely Frenkel pairs without clusters of point defects (unlike the case of cascade damage induced by neutrons and heavy ions) [47].

Self-interstitial atoms exhibit fast one-dimensional diffusion and annihilate at sinks, i.e., free surface and grain boundaries (note that the diffusion of self-interstitial defects occurs at temperatures as low as a few tens of Kelvins [48]) while vacancies remain immobile as their diffusion is activated around 450 K [47, 49]. As a result, the application of recrystallized tungsten foil exposed to 3.5 MeV electron irradiation at room temperature provides PAS samples that are suitable to establish the correlation between the PAS response and concentration of isolated vacancies.

Finally, also samples exposed to controlled plastic deformation were prepared, as positrons are also known to exhibit affinity to dislocations and the deformation induced vacancies. The procedure for the controlled deformation and microstructural characterization is taken from our earlier works [50-52]. Hot-rolled polycrystalline W with a purity of 99.97 wt.% manufactured by Plansee (Austria) was used. A number of dog bone-shaped tensile specimens with an overall length of 120 mm and gauge section dimensions of $50 \times 11 \times 1.1$ mm^3 were cut by EDM from a bar of the material. In order to minimize the initial density of dislocations, grain boundaries, and gaseous impurities, the tensile samples were recrystallized at 1600 °C (just like the foils for electron irradiation) for 1 h in vacuum (0.02 Pa).

To produce specimens with various dislocation densities, interrupted uni-axial tensile tests were carried out. The tensile tests were performed in air at the two temperatures 300 and 600 °C, and up to three different engineering strains: low (3%-5%), medium (20%-22%), and high (36%-38%). The whole gauge section of each sample was homogeneously deformed since no local necking was formed even at the highest applied strain. The initial dislocation density (after 1600 °C annealing) was estimated using TEM as 5×10^{12} m^{-2}. The evolution of the dislocation density with the applied strain was 1×10^{13} - 2×10^{13} - 5×10^{13} m^{-2}, as the deformation

strain reached 3, 20 and 36%, respectively. An in-depth study of the microstructural evolution under controlled plastic deformation in tungsten is reported elsewhere [53].

2.2. Post Irradiation Examination

Positron annihilation spectroscopy (PAS) was used to determine the coincidence Doppler broadening (CDB) spectrum in the irradiated samples. The CDB setup [54-56] consists of two movable high-purity Ge detectors (coaxial HPGe detector from Canberra type GC3018) with high-energy resolution (FWHM = 0.8 keV at 122 keV and FWHM = 1.8 keV at 1332 keV) and build-in preamplifier (model 2101P).

A digital signal processor (DSP Canberra Model 2060) for each detector and personal computer (PC) with LabView acquisition board card were used to collect the spectra. Both the electronics (two detectors and coincidence) as well as the hardware (biological shielding and mobility of the detectors) were optimized to measure highly active specimen with moderate detector dead time (< 20%) and very low background.

The measurements were performed at room temperature using a ^{22}Na positron source. The positron source was sandwiched between two identical samples, such that the fraction of positron annihilations outside the samples is negligible.

The low and high-momentum regions in the CDB spectrum were quantified based on the *S*- and *W*-parameters, respectively. The *S*- and *W*-parameters were defined as the ratio of low momentum ($|c\ p_L| < 2.5 \times 10^{-3}\ m_0 c$) and high momentum ($15 \times 10^{-3}\ m_0 c < |c\ p_L| < 25 \times 10^{-3}\ m_0 c$) regions in the CDB spectrum to the total region, respectively. Here c denotes the lightspeed, m_0 the electron rest mass and p_L the longitudinal component of the positron-electron momentum along the direction of the γ-ray emission.

The micro-hardness was determined using the Reichert-Jung Micro-Duromat 4000 E Vickers hardness test bench. A Vickers indenter was used with a load of 200 g. The load was applied with a load rate of 10 g/s and held for 10 s. The indents were measured via an optical microscope equipped with a digital camera. The calculation of the hardness value follows the ASTM standard E384. For statistics, nine indents per sample were performed randomly across the sample's surface.

2.3. Simulation Method

The irradiation-induced evolution of the microstructure was simulated using the object kinetic Monte Carlo (OKMC) technique. In past works, an in-house developed OKMC code was fine-tuned to reproduce neutron and self-ion irradiation experiments, in a wide dose (0-1 dpa) and temperature range (400-1000 °C) [57-59]. An identical approach is taken in this work, and the most important aspects of the model are briefly summarized in what follows. It is worth noting that no simulations at temperatures higher than 1000 °C were performed, as it goes beyond the calibrated limits of the model.

A cubic OKMC simulation box of size 140×140×140 a_0^3 (i.e. 44.4×44.4×44.4 nm^3) is used and periodic boundary conditions are applied to emulate an infinite material. The minimum resolvable number density (when one single defect is found in the OKMC simulation box) is thus 1.144×10^{22} m^{-3}. However, this number is reduced by an order of magnitude by conducting 10 independent simulations for each irradiation condition.

No grain boundary sinks are defined, while dislocation line sinks are defined with the low density of 10^{10} m^{-2}, consistent with experimental observations (5×10^{7}-3.5×10^{11} m^{-2}, depending on the employed measurement technique) [60]. Additionally, for the sake of computing efficiency, free-migrating self-interstitial atom (cluster) defects are automatically eliminated from the simulation volume after they travelled an equivalent distance of 10 μm in the box without interacting with other point defects. Considering that the latter diffuse one-dimensionally, such cases occur when no other defects are found in their glide cylinder.

Irradiation events are defined accounting for the prescribed dose rate of 10^{-7} dpa/s, consistent with the BR2 reactor conditions. Point defects and their clusters are injected in the simulation box, following predefined catalogues of debris resulting from atomic collision cascades (triggered by impinging neutrons in the material) at the relevant primary knock-on atom energies (see more details in Refs [57-59]).

Once injected in the simulation box, point defects follow simple rules of thermally activated diffusion and mutual interactions, as extensively described in [57-59]. Key parameters are migration energies (accounting for transmutation induced Re), dissociation energies for clusters, and interaction energies with C impurities (whose concentration is set to 20 appm). All underlying interaction parameters were determined based on lower level physical models such as density functional theory and molecular dynamics [61-65].

3. Results

3.1. Coincidence Doppler Broadening

To identify the effect of irradiation temperature on the CDB spectra, I_{irr}, they are normalized against the spectrum of unirradiated single crystal (SC), I_{ref}. The relative CDB spectra, $I_{\mathrm{irr}}/I_{\mathrm{ref}}$, for all investigated irradiation temperatures, T_{irr}, is presented in **Fig. 1**.

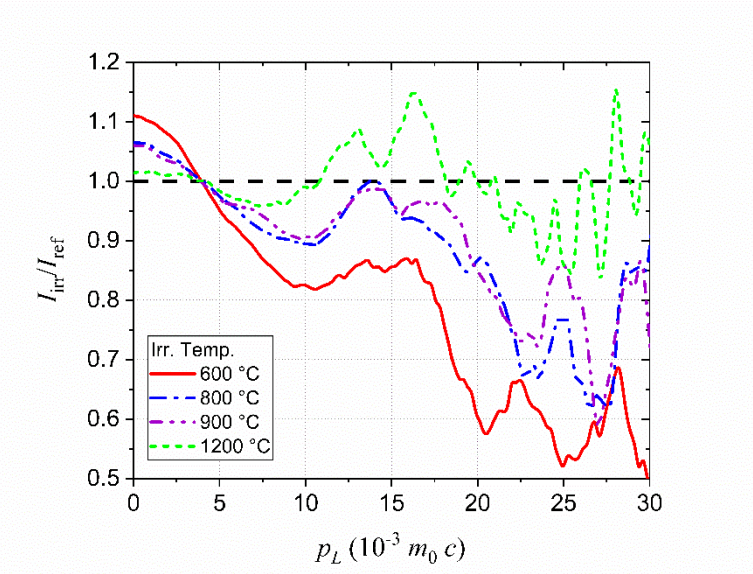

Fig. 1 – Relative CDB spectra, $I_{\mathrm{irr}}/I_{\mathrm{ref}}$, for the investigated irradiation temperatures, T_{irr}.

For T_{irr} in the range 600-900 °C, $I_{\mathrm{irr}}/I_{\mathrm{ref}} > 1$ for $p_L < 4 \times 10^{-3}\, m_0 c$ and $I_{\mathrm{irr}}/I_{\mathrm{ref}} < 1$ for $p_L > 4 \times 10^{-3}\, m_0 c$. A plateau, or slight increase of $I_{\mathrm{irr}}/I_{\mathrm{ref}}$ is observed for $10 \times 10^{-3}\, m_0 c < p_L < 17 \times 10^{-3}\, m_0 c$; and a progressive decrease of $I_{\mathrm{irr}}/I_{\mathrm{ref}}$ above $p_L > 17 \times 10^{-3}\, m_0 c$. This outspoken profile converges to $I_{\mathrm{irr}}/I_{\mathrm{ref}} = 1$ with increasing T_{irr}. In fact, no significant irradiation effects are observed in the CDB spectrum for $T_{\mathrm{irr}} = 1200$ °C.

The CDB profiles observed in this work are fully consistent with the profiles reported by Hu et al [38]. In that work, SC was irradiated in the high flux isotope reactor (HFIR) up to 0.006-0.03 dpa at 90 °C. It is noted that at 90 °C, the profiles are more outspoken with a maximum value for $I_{\mathrm{irr}}/I_{\mathrm{ref}}$ of about 1.3 compared to about 1.1 for $T_{\mathrm{irr}} = 600$ °C in this work. Thus, these data also suggest that $I_{\mathrm{irr}}/I_{\mathrm{ref}}$ converges monotonously to unity with increasing T_{irr} in a wider temperature range than the one investigated in this work.

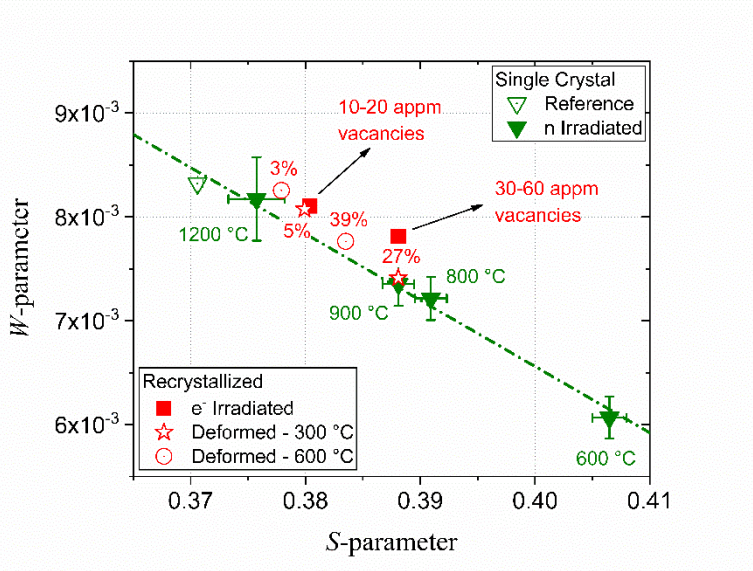

Fig. 2 – S-W plot for the investigated irradiation temperatures, T_{irr}. For comparison, electron irradiated foils and plastically deformed W were added.

In **Fig. 2**, the *S*- and *W*-parameters derived from the CDB spectra are presented in a so-called S-W plot for the different irradiation temperatures, T_{irr}. To signify the impact of the neutron irradiation-induced damage, the values for electron irradiated and plastically deformed W samples are added to the plot. As expected from **Fig. 1**, the *S*-parameter decreases with increasing T_{irr}, while the *W*-parameter increases with T_{irr}. At $T_{\mathrm{irr}} = 1200$ °C, the values for *S*- and *W*-parameter are close to those of the unirradiated sample (reference).

All values for *S*- and *W*-parameter pairs, corresponding to the electron irradiated and plastically deformed samples fall in the range of the neutron irradiated SC in the temperature range 900-1200 °C. For electron irradiation, this corresponds to 10-60 appm of induced vacancies, while for plastic deformation this amounts to 3-39% accumulated (uniform) strain, depending on the deformation temperature. Thus, neutron irradiated SC below 900 °C and an accumulated dose of at least 0.12 dpa induces significantly more open volume damage than the open volume damage induced by typical electron irradiation and plastic deformation. For neutron irradiated SC above 900 °C, the accumulated open volume damage is similar to the open volume damage induced by typical electron irradiation and plastic deformation.

For SC, all data follows a linear trend. This indicates that the formed defects, i.e., vacancy clusters, are: i) not decorated by solute atoms; or ii) the decorating solute atoms are invisible to the PAS-CDB technique. The work by Puska et al [66] reports a positron affinity of -1.31, -0.97, -0.89 and -2.63 eV for W, Re, Os and Ta, respectively. Since only solute-(vacancy) clusters with positron affinity smaller than the host (W) can be observed, the PAS

technique is insensitive to possible (vacancy)ReOs clusters. On the other hand, (vacancy)Ta cluster are observable, but are not detected by PAS due to the very low content of Ta.

It is noted that the electron irradiated and plastically deformed samples follow the same trend. Indeed, it is known that positrons have affinity to both dislocations and vacancies, following the computational studies performed for tungsten [67]. Moreover, for some materials a correlation between the response of PAS to the presence of vacancies and dislocations is established [68]. Based on the present results, for W a certain correlation for the equivalence between the open-volume defects capturing positrons provided by dislocations and isolated vacancies can also be established.

In particular, a concentration of 10-20 appm of isolated vacancies shows the same CDB signal as a dislocation density of ~(1-2)×10^{14} m^{-2}. This could be rather useful information once the detailed investigation of the microstructure of the neutron irradiated samples will be performed by TEM. The latter will hopefully enable the knowledge on the size/density distribution of the nano-cavities and dislocation loops, whose contribution to the PAS signal could then be decoupled thanks to the knowledge of individual contributions coming from isolated vacancies, vacancy clusters [69], voids [69] and line dislocations (based on the correlation established in this work).

3.2. Micro-hardness

The measured irradiation hardening, $\Delta H = H_{\mathrm{irr}} - H_{\mathrm{ref}}$, for all investigated T_{irr} is presented in **Fig. 3**. For comparison, data for single crystal (SC) and polycrystalline (PC) W irradiated up to a similar dose and T_{irr} are added. These data were obtained from irradiation campaigns in the high flux isotope reactor (HFIR) [25] and Japan material testing reactor (JMTR) [21, 26].

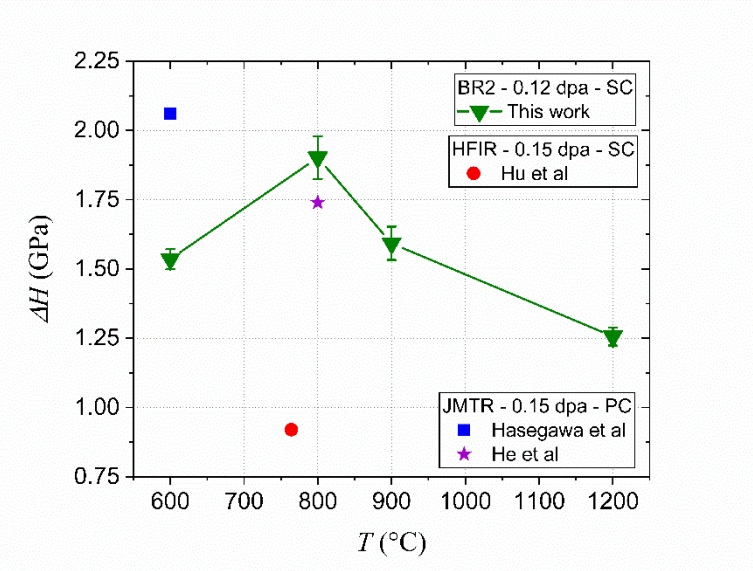

Fig. 3 – Comparison between measured irradiation hardening, ΔH, in this work with values reported in the literature.

For the reference unirradiated sample, the value $H_{\mathrm{ref}} = 3.66 \pm 0.02$ GPa was measured. Our data show a ΔH in the range 1.25-1.90 GPa, which corresponds to a 34-52% increase from H_{ref}. The ΔH increases from 600 to 800 °C and then decreases monotonously up to 1200 °C. Even though the accumulated dose is low, the maximum ΔH at 800 °C is consistent with a peak in void swelling observed ~800 °C [70]. As shown in **Section 3.3** and **Section 4**, the void population with a maximum density at 800 °C can be correlated to ΔH.

However, it is noted that while PAS-CDB data converges to the unirradiated reference for $T_{\mathrm{irr}} = 1200$ °C, there is still significant irradiation-induced hardening. This apparent inconsistency is fully rationalized in **Section 4**.

Except for the data reported by Hu et al [25] (HFIR), our data is in the same range as the reported values in the literature. The large discrepancy in ΔH with Hu et al [25] is possibly due to the large W transmutation rate. In HFIR, starting from pure W, 1.2% Re and 0.08% Os at 0.1 dpa is reported [24], compared to maximal 0.33% Re and 0.10% Os at 0.12 dpa in BR2.

Although no precipitation was observed at this dose [24, 25, 38], the difference in solute concentration can have a significant impact on the resulting irradiation-induced microstructure in terms of void/loop size and density. As discussed in **Section 3.3**, the void and loop density (essentially no loops are observed) reported in [38] is significantly smaller than the ones reported in similar works.

3.3. Object Kinetic Monte Carlo

The results of the OKMC simulations in terms of average void/loop size with diameter, d, and number density, N_D, are presented for T_{irr} in the range 600-1000 °C in **Fig. 4**. For comparison, data for single crystal (SC) and polycrystalline (PC) W irradiated in a similar dose and T_{irr} range are added to the plot. These data were obtained from irradiation campaigns in HFIR [23, 25, 38] and JMTR [21, 26].

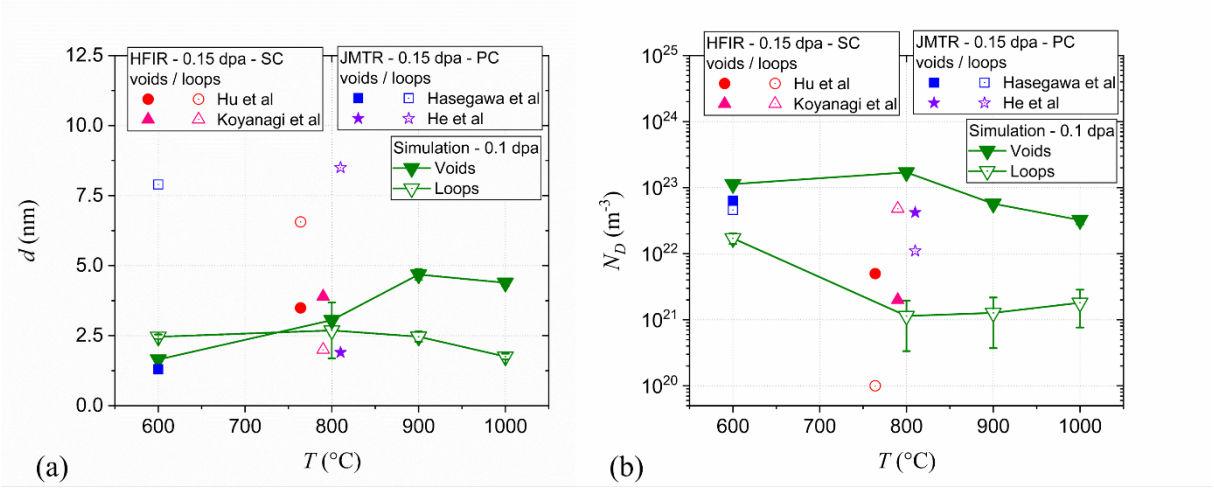

Fig. 4 – Simulated irradiation-induced microstructure in terms of a) average void and loop size, d, and b) average void and loop density, N_D, with T_{irr}. For comparison, data for single crystal (SC) and polycrystalline (PC) W irradiated in a similar dose and T_{irr} range are added to the plot.

The simulations predict that the void size increases from 1.5 to 5 nm with increasing T_{irr}, while the loop size remains constant around 2.5 nm. The void number density exhibits a maximum at 800 °C with $N_D = 2 \times 10^{23}$ m^{-3}, while the loop number density decreases with T_{irr} from $N_D = 2 \times 10^{22}$ m^{-3} down to $N_D = 10^{21}$ m^{-3} for T_{irr} in the range 800-1000 °C. It is noted that $N_D = 10^{21}$ m^{-3} is the lower limit for the present simulation set-up.

The maximum void density at 800 °C is consistent with the reported peak swelling at 800 °C [70]. Following the simulations, below 800 °C the microstructure corresponds to void nucleation and growth (density increase), while above 800 °C the voids coarsen into larger ones and hence the void number density decreases.

The experimental data show large scatter, especially for the defects' number density. While the simulated void size is in excellent agreement with the experimental observations, the

loop size seems somewhat underestimated, when excluding the data point by Koyanagi et al [23]. The latter data point shows an opposite trend, i.e., smaller loop size than void size.

For the defect densities, there is large scatter. Different experiments show opposite trends: Hasegawa et al [21] observes a similar number density of voids and loops, He et al [26] and Hu et al [24] observe a significantly higher void density than loop density (the plotted value for the loop density by Hu et al is an upper bound); and Koyanagi et al [23] observed significantly more loops than voids.

Possible sources for these different observations can be ascribed to different reactors, hence different neutron spectrum and therefore different transmutation rate (as discussed in **Section 3.2**). Even within the same reactor, the neutron spectrum and hence transmutation rate may differ between channels and the precise axial position within the same channel.

Given these differences, it is impossible to make a full quantitative comparison between experiment and simulation. It is clear, however, that the simulated results are within the range of experimental observations.

4. Discussion

In the following, the results from PAS-CDB and micro-hardness are rationalized using simulations and models. The following apparent inconsistencies are addressed: i) increase in void size versus monotonous decrease in S-parameter; ii) a maximum in irradiation hardening versus the monotonous decrease in *S*-parameter; and iii) non-negligible irradiation hardness at 1200 °C versus almost no visible irradiation effects in the CDB spectrum (*S*-parameter).

To explain the evolution of the CDB spectrum and *S*-parameter, it is first noted that while the void density reaches a maximum and decreases above 800 °C, the void size increases monotonically (and saturates). Secondly, it is important to realize that the *S*-parameter is not simply the integrated free volume. While for individual vacancies and small vacancy clusters, the *S*-parameter scales with their integrated volume, i.e. the total number of vacancies, this is not true for large voids. At the center of large voids, the electron density is negligible and hence no electron-positron annihilations can occur. Therefore, it is reasonable to assume that most annihilations occur in the vicinity of the free surface formed by a void.

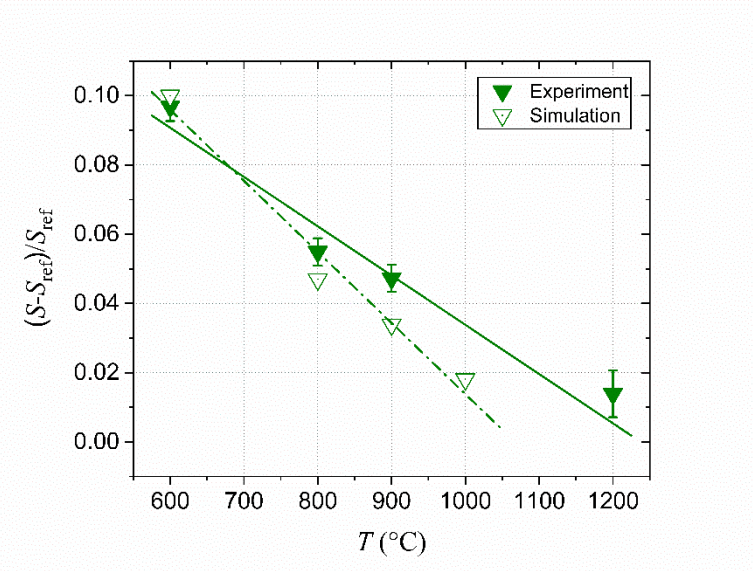

Fig. 5 – Normalized relative difference in *S*-parameter with irradiation temperature from both experiment and simulations.

This effect can be captured by assuming that the contribution of a vacancy cluster containing n vacancies to the *S*-parameter scales as $n^{2/3}$, rather than simply n. Application of these assumptions, i.e., $\Delta S \sim \sum_n n^{2/3}\, N_D(n)$, on the simulated data (see **Fig. 4**) is plotted in **Fig. 5** and compared to the relative *S*-parameter change as obtained from the CDB measurements. Clearly, the simulated ΔS follows a similar linear trend as the experimental data.

It is emphasized that the total integrated volume of vacancy (clusters), $\sum_n n\, N_D(n)$, increases with irradiation temperature. Therefore, the physically based assumption $\Delta S \sim \sum_n n^{2/3}\, N_D(n)$ is essential to explain the evolution of *S*-parameter with irradiation temperature. It is noted that other integration schemes, e.g., a simple cut-off in contribution to ΔS from a certain cluster size, do not respect the linear trend.

Thus, the reduction of *S*-parameter with irradiation temperature is consistent with the increase of vacancy cluster (void) size observed in the simulations. This observation is also consistent with positron annihilation lifetime spectroscopy (PAS-LT) experiments.

PAS-LT results (to be published in a future paper) obtained from SC W(100), irradiated at the same conditions of the present work, show that after irradiation at 600 °C, the average lifetime of positrons increases. As the irradiation temperature increases, the lifetime component of small vacancy (clusters) has the value of that of the unirradiated material, whereas the lifetime component of the largest vacancy complexes is similar for the irradiation temperatures in the range 800-1200 °C.

To rationalize the measured irradiation hardening, it is correlated to the irradiation-induced microstructure via a dispersed barrier model. Thereby the approach similar to the one by Hu et al [25] is followed. Following this theory, the increase in Vickers hardness, ΔH, due to randomly dispersed obstacles can be estimated as,

$$\Delta H = 3.20\, M\alpha\mu b\sqrt{N_D d}, \quad \textbf{(1)}$$

with $M = 3.06$ the Taylor factor, $\mu = 160$ GPa the shear modulus of unirradiated W, $b = 0.272$ nm the Burgers and α the defect obstacle strength. The factor 3.20 correlates the Vickers micro-hardness to the yield strength.

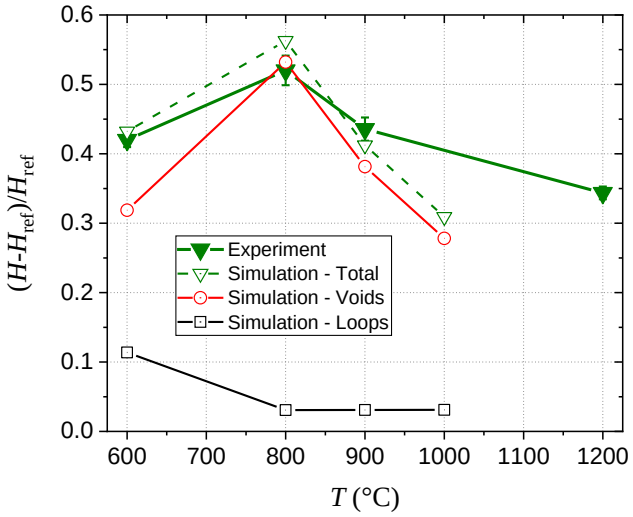

Fig. 6 – The relative irradiation hardening with irradiation temperature from both experiment and simulations.

Equation 1 was applied using the simulated irradiation-induced microstructure (see **Fig. 4**) for both loops and voids, and their total hardening was estimated via linear superposition. A comparison between the simulated and experimental measurements of the relative irradiation hardening is presented in **Fig. 6**. The best fit to the experimental measurements was obtained for $\alpha = 0.2$ for voids and $\alpha = 0.15$ for loops. These values are within the range of the values used by Hu et al [25].

Clearly, the model follows the experimental trend closely, and shows that voids provide the main contribution to the irradiation hardening. Thus, the maximum irradiation hardening at 800 °C can be linked to the maximum void density at 800 °C.

Finally, the observed irradiation hardening, $\Delta H \neq 0$, and $\Delta S \approx 0$ observed at 1200 °C is consistent with picture of a low density of large voids. This is also consistent with PAS-LT (to be published in a future paper) data, where the life time component of large vacancy clusters is still present at 1200 °C, while the component for small vacancy clusters is only present at 600 °C.

5. Conclusions

Single crystal tungsten (W), W(100), was neutron irradiated up to 0.12 dpa in the temperature range 600-1200 °C. The evolution of the vacancy (cluster/void) distribution with irradiation temperature was characterized via PAS-CDB, while the irradiation hardening was measured via micro-mechanical tests. Simulation of the irradiation microstructure combined with application of a dispersed barrier model allowed to link the PAS-CDB observations to the measured irradiation hardening.

It was observed that the CDB spectra converge to the reference one with irradiation temperature, almost coinciding with it at 1200 °C. The derived *S*-parameter decreases linearly with irradiation temperature to almost the reference value at 1200 °C. Simulations of the irradiation-induced microstructure associate this trend to void formation, with increasing void size with irradiation temperature.

Irradiation hardening in the range 34-52% was observed at all irradiation temperatures, with a maximum at 800 °C. Application of a dispersed barrier model linked the peak hardening to the peak density of voids and showed that voids are responsible to the main contribution of the irradiation hardening.

The observed irradiation hardening of 32% at 1200 °C and recovery of *S*-parameter can be linked to an irradiation microstructure dominated by a low density of large voids.

Acknowledgements

This work has been carried out within the framework of the EUROfusion Consortium and has received funding from the Euratom research and training programme 2014-2018 and 2019-2020 under grant agreement No. 633053. The views and opinions expressed herein do not necessarily reflect those of the European Commission.

References

[1] F.E. Roadmap, https://www.euro-fusion.org/fileadmin/user_upload/EUROfusion/Documents/2018_Research_roadmap_long_version_01.pdf (2018).
[2] D. Stork, P. Agostini, J.L. Boutard, D. Buckthorpe, E. Diegele, S.L. Dudarev, C. English, G. Federici, M.R. Gilbert, S. Gonzalez, A. Ibarra, C. Linsmeier, A. Li Puma, G. Marbach, P.F. Morris, L.W. Packer, B. Raj, M. Rieth, M.Q. Tran, D.J. Ward, S.J. Zinkle, Developing structural, high-heat flux and plasma facing materials for a near-term DEMO fusion power plant: The EU assessment, J Nucl Mater 455(1-3) (2014) 277-291.
[3] D. Maisonnier, I. Cook, S. Pierre, B. Lorenzo, D.P. Luigi, G. Luciano, N. Prachai, P. Aldo, DEMO and fusion power plant conceptual studies in Europe, Fusion Engineering and Design 81(8-14) (2006) 1123-1130.
[4] G. Federici, W. Biel, M.R. Gilbert, R. Kemp, N. Taylor, R. Wenninger, European DEMO design strategy and consequences for materials, Nuclear Fusion 57(9) (2017).
[5] G. Pintsuk, Tungsten as plasma facing material, Comprehensive Nuclear Materials 4 (2012) 551-581.
[6] A. Giannattasio, Z. Yao, E. Tarleton, S.G. Roberts, Brittle–ductile transitions in polycrystalline tungsten, Philosophical Magazine 90 (2010) 3947-3959.
[7] J.M. Steichen, Tensile Properties of Neutron-Irradiated Tzm and Tungsten, Journal of Nuclear Materials 60(1) (1976) 13-19.
[8] I.V. Gorynin, V.A. Ignatov, V.V. Rybin, S.A. Fabritsiev, V.A. Kazakov, V.P. Chakin, V.A. Tsykanov, V.R. Barabash, Y.G. Prokofyev, Effects of Neutron-Irradiation on Properties of Refractory-Metals, Journal of Nuclear Materials 191 (1992) 421-425.
[9] I. Alexandrov, I.V. Gorynin, Metallovedenie 22 (1979) 35.
[10] T. Tanno, M. Fukuda, S. Nogami, A. Hasegawa, Microstructure Development in Neutron Irradiated Tungsten Alloys, MATERIALS TRANSACTIONS 52(7) (2011) 1447-1451.
[11] D. Terentyev, P. Grammatikopoulos, D. Bacon, Y. Osetsky, Simulation of the interaction between an edge dislocation and a <100> interstitial dislocation loop in α-iron, Acta Materialia 56 (2008) 5034-5046.
[12] D. Terentyev, D. Bacon, Y. Osetsky, Interaction of an edge dislocation with voids in a-iron modelled with different interatomic potentials, Journal of Physics: Condensed Matter 20 (2008) 445007.
[13] D.A. Terentyev, Y.N. Osetsky, D.J. Bacon, Effects of temperature on structure and mobility of the < 1 0 0 > edge dislocation in body-centred cubic iron, Acta Materialia 58(7) (2010) 2477-2482.
[14] S. Brezinsek, J.W. Coenen, T. Schwarz-Selinger, K. Schmid, A. Kirschner, A. Hakola, F.L. Tabares, H.J. van der Meiden, M.L. Mayoral, M. Reinhart, E. Tsitrone, T. Ahlgren, M. Aints, M. Airila, S.

Almaviva, E. Alves, T. Angot, V. Anita, R.A. Parra, F. Aumayr, M. Balden, J. Bauer, M. Ben Yaala, B.M. Berger, R. Bisson, C. Bjorkas, I.B. Radovic, D. Borodin, J. Bucalossi, J. Butikova, B. Butoi, I. Cadez, R. Caniello, L. Caneve, G. Cartry, N. Catarino, M. Cekada, G. Ciraolo, L. Ciupinski, F. Colao, Y. Corre, C. Costin, T. Craciunescu, A. Cremona, M. De Angeli, A. de Castro, R. Dejarnac, D. Dellasega, P. Dinca, T. Dittmar, C. Dobrea, P. Hansen, A. Drenik, T. Eich, S. Elgeti, D. Falie, N. Fedorczak, Y. Ferro, T. Fornal, E. Fortuna-Zalesna, L. Gao, P. Gasior, M. Gherendi, F. Ghezzi, Z. Gosar, H. Greuner, E. Grigore, C. Grisolia, M. Groth, M. Gruca, J. Grzonka, J.P. Gunn, K. Hassouni, K. Heinola, T. Hoschen, S. Huber, W. Jacob, I. Jepu, X. Jiang, I. Jogi, A. Kaiser, J. Karhunen, M. Kelemen, M. Koppen, H.R. Koslowski, A. Kreter, M. Kubkowska, M. Laan, L. Laguardia, A. Lahtinen, A. Lasa, V. Lazic, N. Lemahieu, J. Likonen, J. Linke, A. Litnovsky, C. Linsmeier, T. Loewenhoff, C. Lungu, M. Lungu, G. Maddaluno, H. Maier, T. Makkonen, A. Manhard, Y. Marandet, S. Markelj, L. Marot, C. Martin, A.B. Martin-Rojo, Y. Martynova, R. Mateus, D. Matveev, M. Mayer, G. Meisl, N. Mellet, A. Michau, J. Miettunen, S. Moller, T.W. Morgan, J. Mougenot, M. Mozetic, V. Nemanic, R. Neu, K. Nordlund, M. Oberkofler, E. Oyarzabal, M. Panjan, C. Pardanaud, P. Paris, M. Passoni, B. Pegourie, P. Pelicon, P. Petersson, K. Piip, G. Pintsuk, G.O. Pompilian, G. Popa, C. Porosnicu, G. Primc, M. Probst, J. Raisanen, M. Rasinski, S. Ratynskaia, D. Reiser, D. Ricci, M. Richou, J. Riesch, G. Riva, M. Rosinski, P. Roubin, M. Rubel, C. Ruset, E. Safi, G. Sergienko, Z. Siketic, A. Sima, B. Spilker, R. Stadlmayr, I. Steudel, P. Strom, T. Tadic, D. Tafalla, I. Tale, D. Terentyev, A. Terra, V. Tiron, I. Tiseanu, P. Tolias, D. Tskhakaya, A. Uccello, B. Unterberg, I. Uytdenhoven, E. Vassallo, P. Vavpetic, P. Veis, I.L. Velicu, J.W.M. Vernimmen, A. Voitkans, U. von Toussaint, A. Weckmann, M. Wirtz, A. Zaloznik, R. Zaplotnik, W.P. Contributors, Plasma-wall interaction studies within the EUROfusion consortium: progress on plasma-facing components development and qualification, Nuclear Fusion 57(11) (2017).

[15] J. Habainy, Y. Dai, Y. Lee, S. Iyengar, Thermal diffusivity of tungsten irradiated with protons up to 5.8 dpa, Journal of Nuclear Materials 509 (2018) 152-157.

[16] S. Markelj, O.V. Ogorodnikova, P. Pelicon, T.S. Selinger, P. Vavpetic, I. Cadez, In situ nuclear reaction analysis of D retention in undamaged and self-damaged tungsten under atomic D exposure, Physica Scripta T159 (2014).

[17] O.V. Ogorodnikova, K. Sugiyama, Effect of radiation-induced damage on deuterium retention in tungsten, tungsten coatings and Eurofer, Journal of Nuclear Materials 442(1-3) (2013) 518-527.

[18] M. Fukuda, T. Tanno, S. Nogami, A. Hasegawa, Effects of Re Content and Fabrication Process on Microstructural Changes and Hardening in Neutron Irradiated Tungsten, Materials Transactions 53(12) (2012) 2145-2150.

[19] A. Hasegawa, M. Fukuda, S. Nogami, K. Yabuuchi, Neutron irradiation effects on tungsten materials, Fusion Eng Des 89(7-8) (2014) 1568-1572.

[20] A. Hasegawa, M. Fukuda, K. Yabuuchi, S. Nogami, Neutron irradiation effects on the microstructural development of tungsten and tungsten alloys, Journal of Nuclear Materials 471 (2016) 175-183.
[21] A. Hasegawa, M. Fukuda, T. Tanno, S. Nogami, Neutron Irradiation Behavior of Tungsten, Materials Transactions 54(4) (2013) 466-471.
[22] M. Fukuda, K. Yabuuchi, S. Nogami, A. Hasegawa, T. Tanaka, Microstructural development of tungsten and tungsten–rhenium alloys due to neutron irradiation in HFIR, Journal of Nuclear Materials 455(1) (2014) 460-463.
[23] T. Koyanagi, N.A.P.K. Kumar, T. Hwang, L.M. Garrison, X. Hu, L.L. Snead, Y. Katoh, Microstructural evolution of pure tungsten neutron irradiated with a mixed energy spectrum, Journal of Nuclear Materials 490 (2017) 66-74.
[24] X. Hu, C.M. Parish, K. Wang, T. Koyanagi, B.P. Eftink, Y. Katoh, Transmutation-induced precipitation in tungsten irradiated with a mixed energy neutron spectrum, Acta Mater. 165 (2019) 51-61.
[25] X. Hu, T. Koyanagi, M. Fukuda, N.A.P.K. Kumar, L.L. Snead, B.D. Wirth, Y. Katoh, Irradiation hardening of pure tungsten exposed to neutron irradiation, Journal of Nuclear Materials 480 (2016) 235-243.
[26] J.C. He, G.Y. Tang, A. Hasegawa, K. Abe, Microstructural development and irradiation hardening of W and W–(3–26) wt%Re alloys after high-temperature neutron irradiation to 0.15 dpa, Nuclear Fusion 46(11) (2006) 877-883.
[27] X.X. Hu, C.M. Parish, K. Wang, T. Koyanagi, B.P. Eftink, Y. Katoh, Transmutation-induced precipitation in tungsten irradiated with a mixed energy neutron spectrum, Acta Materialia 165 (2019) 51-61.
[28] Y. Katoh, L.L. Snead, L.M. Garrison, X. Hu, T. Koyanagi, C.M. Parish, P.D. Edmondson, M. Fukuda, T. Hwang, T. Tanaka, A. Hasegawa, Response of unalloyed tungsten to mixed spectrum neutrons, Journal of Nuclear Materials 520 (2019) 193-207.
[29] M.H. Cui, T.L. Shen, H.P. Zhu, J. Wang, X.Z. Cao, P. Zhang, L.L. Pang, C.F. Yao, K.F. Wei, Y.B. Zhu, B.S. Li, J.R. Sun, N. Gao, X. Gao, H.P. Zhang, Y.B. Sheng, H.L. Chang, W.H. He, Z.G. Wang, Vacancy like defects and hardening of tungsten under irradiation with He ions at 800°C, Fusion Eng Des 121 (2017) 313-318.
[30] A. Debelle, M.F. Barthe, T. Sauvage, First temperature stage evolution of irradiation-induced defects in tungsten studied by positron annihilation spectroscopy, Journal of Nuclear Materials 376(2) (2008) 216-221.

[31] J. Heikinheimo, K. Mizohata, J. Räisänen, T. Ahlgren, P. Jalkanen, A. Lahtinen, N. Catarino, E. Alves, F. Tuomisto, Direct observation of mono-vacancy and self-interstitial recovery in tungsten, 7(2) (2019) 021103.
[32] Y.L. Liu, E.Y. Lu, L.G. Song, R.Y. Bai, Q. Xu, S.X. Jin, T. Zhu, X.Z. Cao, Q.L. Zhang, D.Q. Yuan, B.Y. Wang, L.Q. Ge, Depth synergistic effect of irradiation damage on tungsten irradiated by He-ions with various energies, Journal of Nuclear Materials 517 (2019) 192-200.
[33] F. Liu, C. Zhang, C. He, H.-S. Zhou, F. Ding, G.-N. Luo, Characterization of radiation defects in quasi-homogeneously damaged tungsten by PALS and TEM, Nuclear Instruments and Methods in Physics Research Section B: Beam Interactions with Materials and Atoms 439 (2019) 17-21.
[34] O.V. Ogorodnikova, L.Y. Dubov, S.V. Stepanov, D. Terentyev, Y.V. Funtikov, Y.V. Shtotsky, V.S. Stolbunov, V. Efimov, K. Gutorov, Annealing of radiation-induced defects in tungsten: Positron annihilation spectroscopy study, Journal of Nuclear Materials 517 (2019) 148-151.
[35] O.V. Ogorodnikova, M. Majerle, V.V. Gann, J. Čížek, P. Hruška, S. Simakov, M. Štefánik, V. Zach, Verification of the theory of primary radiation damage by comparison with experimental data, Journal of Nuclear Materials 525 (2019) 22-31.
[36] W. Qin, S. Jin, X. Cao, Y. Wang, P. Peres, S.-Y. Choi, C. Jiang, F. Ren, Influence of nanochannel structure on helium-vacancy cluster evolution and helium retention, Journal of Nuclear Materials 527 (2019) 151822.
[37] I. Uytdenhouwen, T. Schwarz-Selinger, J.W. Coenen, M. Wirtz, Mechanical and microstructural changes in tungsten due to irradiation damage, Physica Scripta T167 (2016) 014007.
[38] X. Hu, T. Koyanagi, M. Fukuda, Y. Katoh, L.L. Snead, B.D. Wirth, Defect evolution in single crystalline tungsten following low temperature and low dose neutron irradiation, Journal of Nuclear Materials 470 (2016) 278-289.
[39] C.N. Taylor, M. Shimada, B.J. Merrill, M.W. Drigert, D.W. Akers, Y. Hatano, Development of positron annihilation spectroscopy for characterizing neutron irradiated tungsten, Physica Scripta T159 (2014) 014055.
[40] C.N. Taylor, M. Shimada, B.J. Merrill, D.W. Akers, Y. Hatano, Development of positron annihilation spectroscopy for investigating deuterium decorated voids in neutron-irradiated tungsten, Journal of Nuclear Materials 463 (2015) 1009-1012.
[41] D.B. Pelowitz, J.W. Durkee, J.S. Elson, M.L. Fensin, J.S. Hendricks, M.R. James, R.C. Johns, G.W. Mc Kinney, S.G. Mashnik, L.S. Waters, T.A. Wilcox, J.M. Verbeke, MCNPX 2.7.0 extensions, ; Los Alamos National Lab. (LANL), Los Alamos, NM (United States), 2011, p. Medium: ED.
[42] M.J. Norgett, M.T. Robinson, I.M. Torrens, A proposed method of calculating displacement dose rates, Nuclear Engineering and Design 33(1) (1975) 50-54.

[43] K.S. Nordlund, A. E.; Granberg, F.; Zinkle, S. J.; Stoller, R.; Averback, R. S.; Suzudo, T.; Malerba, L.; Banhart, F.; Weber, W. J.; Willaime, F.; Dudarev, S.; Simeone, D., Primary Radiation Damage in Materials, Nuclear Energy Agency, 2015.
[44] A. Stankovskiy, G. Van Den Eynde, P. Baeten, C. Trakas, P.M. Demy, L. Villatte, ALEPH2 - A general purpose Monte Carlo depletion code, American Nuclear Society - ANS; La Grange Park, IL (United States); American Nuclear Society, Inc., 555 N. Kensington Avenue, La Grange Park, Illinois 60526 (United States)2012.
[45] A.Y. Konobeyev, U. Fischer, Y.A. Korovin, S.P. Simakov, Evaluation of effective threshold displacement energies and other data required for the calculation of advanced atomic displacement cross-sections, Nuclear Energy and Technology 3(3) (2017) 169-175.
[46] O.S. Oen, Cross sections for atomic displacements in solids by fast electrons, ; Oak Ridge National Lab., Tenn. (USA), 1973, p. Medium: ED; Size: Pages: 207.
[47] H.H. Neely, D.W. Keefer, A. Sosin, Electron Irradiation and Recovery of Tungsten, Phys. Stat. Sol. 28 (1968) 675-682.
[48] T. Amino, K. Arakawa, H. Mori, Activation energy for long-range migration of self-interstitial atoms in tungsten obtained by direct measurement of radiation-induced point-defect clusters, Philosophical Magazine Letters 91(2) (2011) 86-96.
[49] L.K. Keys, J.P. Smith, J. Moteff, High-Temperature Recovery of Tungsten after Neutron Irradiation, Physical Review 176 (1968) 851-856.
[50] D. Terentyev, G. De Temmerman, B. Minov, Y. Zayachuk, K. Lambrinou, T.W. Morgan, A. Dubinko, K. Bystrov, G. Van Oost, Synergy of plastic deformation and gas retention in tungsten, Nuclear Fusion 55(1) (2015) 013007.
[51] D. Terentyev, G. De Temmerman, T.W. Morgan, Y. Zayachuk, K. Lambrinou, B. Minov, A. Dubinko, K. Bystrov, G. Van Oost, Effect of plastic deformation on deuterium retention and release in tungsten, J Appl Phys 117(8) (2015) 083302.
[52] M. Zibrov, M. Balden, M. Dickmann, A. Dubinko, W. Egger, M. Mayer, D. Terentyev, M. Wirtz, Deuterium trapping by deformation-induced defects in tungsten, Nuclear Fusion 59(10) (2019).
[53] A. Dubinko, D. Terentyev, A. Bakaeva, K. Verbeken, M. Wirtz, M. Hernandez-Mayoral, Evolution of plastic deformation in heavily deformed and recrystallized tungsten of ITER specification studied by TEM, Int. Journal of Refractory Metals and Hard Materials 66 (2017) 105-115.
[54] K. Verheyen, M. Jardin, A. Almazouzi, Coincidence Doppler broadening spectroscopy in Fe, Fe–C and Fe–Cu after neutron irradiation, Journal of Nuclear Materials 351(1) (2006) 209-215.
[55] M.J. Konstantinović, G. Bonny, Thermal stability and the structure of vacancy-solute clusters in iron alloys, Acta Mater. 85 (2015) 107-111.

[56] M.J. Konstantinović, I. Uytdenhouwen, G. Bonny, N. Castin, L. Malerba, P. Efsing, Radiation induced solute clustering in high-Ni reactor pressure vessel steel, Acta Mater. 179 (2019) 183-189.
[57] N. Castin, A. Bakaev, G. Bonny, A.E. Sand, L. Malerba, D. Terentyev, On the onset of void swelling in pure tungsten under neutron irradiation: An object kinetic Monte Carlo approach, Journal of Nuclear Materials 493 (2017) 280-293.
[58] N. Castin, G. Bonny, A. Bakaev, C.J. Ortiz, A.E. Sand, D. Terentyev, Object kinetic Monte Carlo model for neutron and ion irradiation in tungsten: Impact of transmutation and carbon impurities, Journal of Nuclear Materials 500 (2018) 15-25.
[59] N. Castin, A. Dubinko, G. Bonny, A. Bakaev, J. Likonen, A. De Backer, A.E. Sand, K. Heinola, D. Terentyev, The influence of carbon impurities on the formation of loops in tungsten irradiated with self-ions, Journal of Nuclear Materials 527 (2019) 151808.
[60] V. Glebovsky, B. Sergey, Tungsten Single Crystals of High Structural Quality, 2009.
[61] G. Bonny, N. Castin, A. Bakaev, D. Terentyev, Kinetic Monte Carlo model for 1-D migration in a field of strong traps: Application to self-interstitial clusters in W-Re alloys, Computational Materials Science 144 (2018) 355-362.
[62] A. Bakaev, A. Zinovev, D. Terentyev, G. Bonny, C. Yin, N. Castin, Y.A. Mastrikov, E.E. Zhurkin, Interaction of carbon with microstructural defects in a W-Re matrix: An ab initio assessment, Journal of Applied Physics 126(7) (2019) 075110.
[63] A.E. Sand, S.L. Dudarev, K. Nordlund, High-energy collision cascades in tungsten: Dislocation loops structure and clustering scaling laws, EPL 103(4) (2013) 46003.
[64] A.E. Sand, K. Nordlund, S.L. Dudarev, Radiation damage production in massive cascades initiated by fusion neutrons in tungsten, Journal of Nuclear Materials 455(1) (2014) 207-211.
[65] N. Castin, P. Dwivedi, L. Messina, A. Bakaev, D. Terentyev, G. Bonny, The effect of rhenium on the diffusion of small interstitial clusters in tungsten, Computational Materials Science 177 (2020) 109580.
[66] M.J. Puska, P. Lanki, R.M. Nieminen, Positron affinities for elemental metals, Journal of Physics: Condensed Matter 1(35) (1989) 6081-6094.
[67] P. Staikov, N. Djourelov, Simulations of < 1 0 0 > edge and 1/2 < 1 1 1 > screw dislocations in alpha-iron and tungsten and positron lifetime calculations, Physica B-Condensed Matter 413 (2013) 59-63.
[68] J.B. Pang, H. Li, K. Zhou, Z. Wang, The Correlation Between Dislocations and Vacancy Defects Using Positron Annihilation Spectroscopy, Plasma Sci Technol 14(7) (2012) 650-655.
[69] T. Troev, E. Popov, P. Staikov, N. Nankov, T. Yoshiie, Positron simulations of defects in tungsten containing hydrogen and helium, Nucl Instrum Meth B 267(3) (2009) 535-541.

[70] J. Matolich, H. Nahm, J. Moteff, Swelling in neutron irradiated tungsten and tungsten-25 percent rhenium, Scripta Metallurgica 8(7) (1974) 837-841.